

Convergence Analysis of a Steerable Nip Mechanism for Full Sheet Control in Printing Devices

Edgar Ergueta

e-mail: edgar.ergueta@wdc.com

Rene Sanchez

e-mail: r2sanchez@gmail.com

Roberto Horowitz

e-mail: horowitz@me.berkeley.edu

Masayoshi Tomizuka

e-mail: tomizuka@me.berkeley.edu

Department of Mechanical Engineering,
University of California,
Berkeley, CA 94720

Current approaches for high speed color printers require sheets be accurately positioned as they arrive to the image transfer station (ITS). This goal has been achieved by designing and building a steerable nip mechanism, which is located upstream from the ITS. This mechanism consists of two rollers that not only rotate to advance the paper along the track, but also steer the paper in the yaw direction. This paper briefly reviews the design and experimental setup of the system, and focuses on the design and analysis of a controller that precisely corrects the lateral, longitudinal, and angular positions of the sheet. The control strategy used is based on linearization by state feedback with the addition of internal loops for the local control of the actuators. This paper also provides a methodology to tune the controller parameters so that the desired performance specifications are met. The success of this mechatronic approach is corroborated through simulation and experimental results, which show that the system is able to correct sheet errors and meet all the performance specifications. [DOI: 10.1115/1.3117195]

1 Introduction

Current approaches for paper path control require sheets to be accurately positioned as they arrive to the image transfer station (ITS). This is achieved by using a registration device, located between the paper path and the ITS, which not only corrects for longitudinal, lateral, and angular errors, but also delivers the sheet on time to the ITS. Prior work on sheet control in a printer paper path has been mainly focused in developing control techniques for coordinating multiple actuated sections of the paper path, in order to correct for longitudinal interspersing errors among sheets, and synchronize the arrival of sheets to the ITS with its corresponding image [1–7]. Other works, such as in Refs. [8–12], do consider the sheet's lateral and skew position error corrections, but they fail to do so at large speeds and without marking the page. In this paper we present the control architecture of a mechatronic solution that corrects for sheet position errors at high speeds without damaging the page. This is achieved by using the steerable nip mechanism [13] depicted in Fig. 1, whose design is described in detail in Refs. [14–16].

The problem of controlling paper trajectories with steerable nips is similar to the control of two-wheel robots, such as the one studied in Ref. [17]. However, not only does the two-wheel robot have one less degree of freedom than the steerable nip system, but also the control law proposed by Yun and Sarkar [17] fails to account for singularities that arise when the steering angle of the wheels approaches zero. Moreover, in the case of the two-wheel robot, three inputs are needed to follow a reference trajectory. This is not the case with steerable nips, where four inputs are needed due to the flexibility of the paper; two inputs rotate and steer roller 1, whereas the other two inputs do the same for roller 2 (see Fig. 1).

Similar to the two-wheel robot, the steerable nip mechanism is a nonlinear system with nonholonomic constraints. For the steerable nip system, two nonholonomic constraints come from nonslip conditions on the rollers, and the other two come from local ve-

locities (of the paper) being zero in the direction perpendicular to the rotation of the rollers. Additional details on the constraints of this particular system can be found in Ref. [14].

The control objective of the steerable nip device consists of correcting the position of the sheet on a horizontal plane while the sheet is moving in the longitudinal direction at all times. Since the page should move without getting damaged, it is also necessary to control the sheet's amount of buckling. The control strategy used to achieve these goals is based on state feedback linearization [18] with inner loops for the control of the roller's rotational angular velocity and steering angular position. Recently, Elliot and Gans [19] presented a control strategy for an underactuated steerable nip mechanism for printer sheet registration devices similar to the device described in this paper. However, since this mechanism does not consider the sheet's amount of buckling, it has one less degree of freedom than the mechanism presented in this paper. Thus, the control problem described in Ref. [19] resembles more than that of the two-wheel robot in Ref. [17], and the control strategy presented there is significantly different from the one we present.

The remainder of this paper is organized as follows. Section 2 briefly describes the steerable nip section and the experimental setup. Section 3 presents the mathematical model of the system. Sections 4 and 5 describe the control strategy and convergence analysis for the closed-loop system, respectively. Section 6 presents the methodology proposed to tune the controller gains. Simulation and experimental results are shown in Sec. 7. Finally, conclusions are stated in Sec. 8.

2 Experimental Setup

The steerable nip mechanism has been designed so that it can correct for sheet lateral position errors without having to move the actuators and without inflicting any damage on the page. This has been achieved by steering two rollers, which are underneath two backer balls. As seen in Fig. 2, each roller is driven by a servomotor (referred as *process direction actuator*) attached to a rotating table, which is in turn steered by another servomotor (referred as *steering actuator*) through a coupling. The sheet moves along a flat surface, and passes between the two backer balls and rollers, as shown in Figs. 2 and 3; note that the page moves in the direction of the arrow labeled v .

Figure 4 is a photograph of the experimental system we have

Contributed by the Dynamic Systems, Measurement, and Control Division of ASME for publication in the JOURNAL OF DYNAMIC SYSTEMS, MEASUREMENT, AND CONTROL. Manuscript received December 12, 2007; final manuscript received February 17, 2009; published online December 9, 2009. Assoc. Editor: Robert Gao.

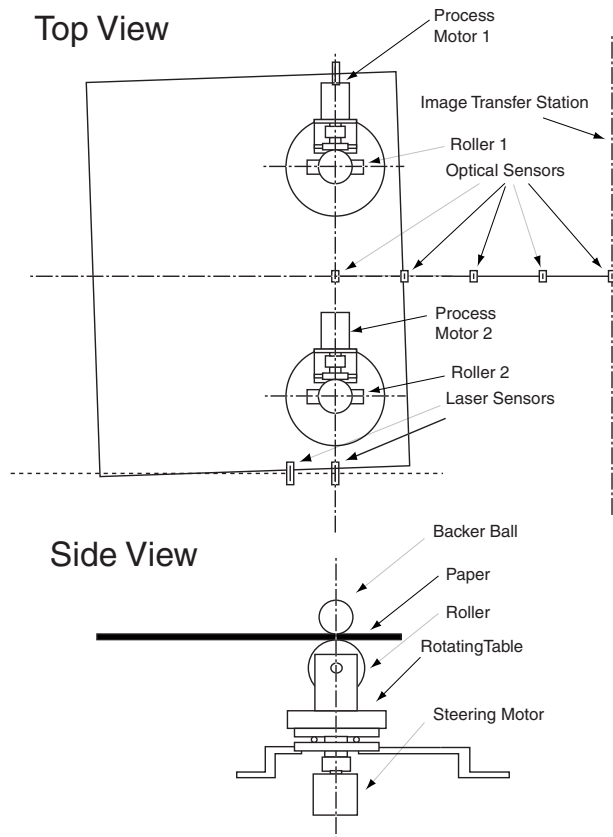


Fig. 1 Schematic of steerable nip fixture

built. As shown in Fig. 4, the page is delivered to the steerable nip section by a feeder unit (located at the back of the picture). Then, while the page moves on top of the horizontal plate, its position is being corrected by the steerable nip mechanism, which is located below the plate; a photograph of the dc motors driving the rollers is shown in Fig. 5. Finally, the sheet is removed through an exit roller (located at the front of the picture). It is assumed that the location of the exit roller in the experimental setup is the location of the entrance to the ITS. Thus, the performance of the controller is determined by the position and orientation of the paper as it arrives to the exit roller.

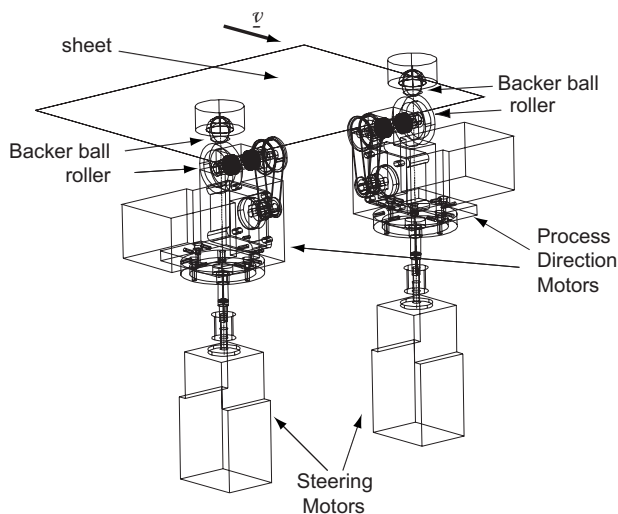


Fig. 2 Sheet moving through the steerable nip mechanism

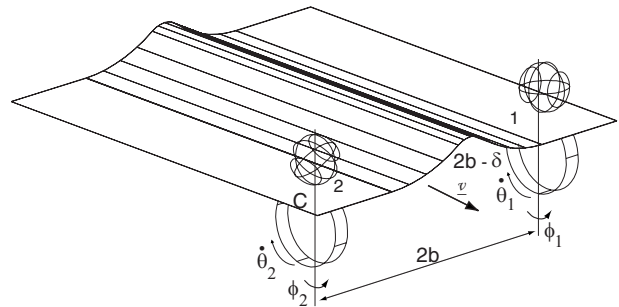


Fig. 3 Steerable nips with paper buckle

In order to determine the position, orientation, and the amount of buckling of the sheet, it is necessary to detect the edges of the page. As seen in Fig. 1, two laser sensors are located on the right hand side of the page, which are used to measure the lateral and angular positions of the page. Furthermore, to measure the longitudinal position of the page, five single photodiode (optical) sensors, spaced 52 mm apart, are located along the process direction. It should be noticed that whereas we are able to obtain continuous measurements for lateral and angular positions of the sheet, we need to estimate its longitudinal position when the leading edge of the page is between two consecutive photodiodes. In this paper we

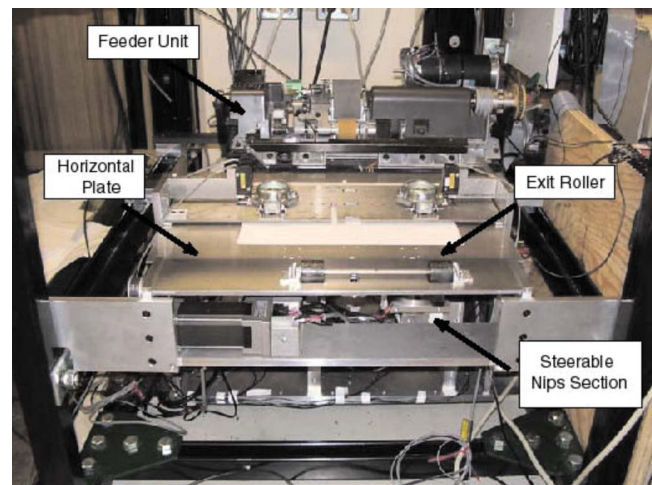


Fig. 4 Experimental setup

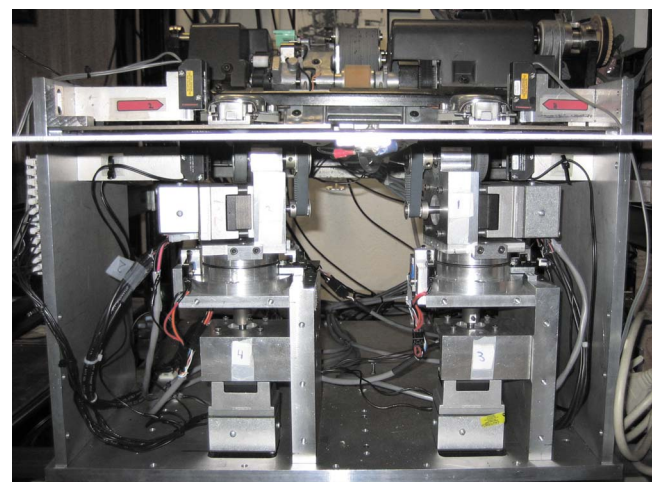


Fig. 5 DC motors used for the steerable nip mechanism

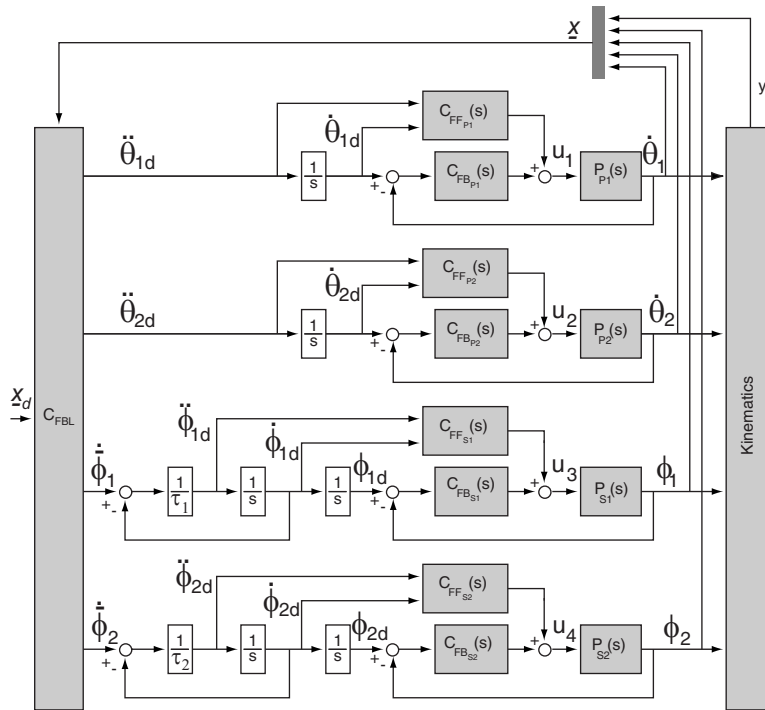


Fig. 6 System block diagram for implemented system

estimate longitudinal position through the use of an open-loop observer based on the kinematic relations described in Sec. 3. The same observer is used to estimate the amount of buckling of the sheet.

3 System Model

As described in Fig. 3, the steerable nip mechanism has two independent steering rollers located at points 1 and 2, which are separated by a distance $2b$. The space-fixed coordinates of the system (x, y, ϕ, δ) locate the leading right corner of the sheet, point C , which will be used to track the position of the page. Note that x, y , and ϕ are the lateral, longitudinal, and angular positions of the sheet, respectively. The amount of buckling, δ , is defined as the difference between the distance separating points 1 and 2, as measured along the paper, $2b - \delta$, and along the straight line, $2b$ (see Fig. 3). Thus, a negative δ represents the amount of buckling on a sheet, whereas a positive δ occurs when the paper stretches; stretching needs to be avoided at all times. Also note that the origin $(0,0)$ of the space-fixed frame is located in the middle of points 1 and 2. Furthermore, $\dot{\theta}_i$ represents the angular velocity of the rollers in the direction parallel to the sheet, and $\dot{\phi}_i$ represents their angular position in the direction perpendicular to the sheet (for $i=1, 2$).

The kinematic model of the system is derived so that the four nonholonomic constraints mentioned in Sec. 1 are satisfied at all times. This model, whose complete derivation can be found in Refs. [15,16], is represented by the following equations:

$$\dot{x} = -\frac{r_1 y}{2b} \cos \phi_1 \dot{\theta}_1 + r_2 \left(\frac{y}{2b} \cos \phi_2 + \sin \phi_2 \right) \dot{\theta}_2 \quad (1)$$

$$\dot{y} = \frac{r_1(x-b)}{2b} \cos \phi_1 \dot{\theta}_1 - \frac{r_2(x+b)}{2b} \cos \phi_2 \dot{\theta}_2 \quad (2)$$

$$\dot{\phi} = \frac{1}{2b} (r_1 \cos \phi_1 \dot{\theta}_1 - r_2 \cos \phi_2 \dot{\theta}_2) \quad (3)$$

$$\dot{\delta} = r_2 \sin \phi_2 \dot{\theta}_2 - r_1 \sin \phi_1 \dot{\theta}_1 \quad (4)$$

where r_1 and r_2 are the radii of the two rollers. As mentioned in Refs. [15,16], a simple model that adequately describes both the process direction and steering actuator dynamics is given by

$$\ddot{\theta}_i + \alpha_{pi} \dot{\theta}_i = \beta_{pi} V_{pi} \quad (i=1,2) \quad (5)$$

$$\ddot{\phi}_i + \alpha_{si} \dot{\phi}_i = \beta_{si} V_{si} \quad (i=1,2) \quad (6)$$

where V_{ji} is the voltage input to the motor, and α_{ji} and β_{ji} are actuator coefficients that depend on the inertias and rotational viscous damping coefficients of the different components of the steerable nip mechanism; subindices p and s stand for process direction and steering actuators, respectively, and subindex i corresponds to each of the two rollers.

The complete dynamic system model is composed of Eqs. (1)–(6). We can further define the state vector as $\underline{x} = [x \ y \ \phi \ \delta \ \phi_1 \ \phi_2 \ \dot{\theta}_1 \ \dot{\theta}_2 \ \dot{\phi}_1 \ \dot{\phi}_2]^T$, the input vector as $\underline{u} = [u_1 \ u_2 \ u_3 \ u_4]^T = [V_{p1} \ V_{p2} \ V_{s1} \ V_{s2}]^T$, and the output vector as $\underline{y} = [x \ y \ \phi \ \delta]^T$.

4 Control Strategy

The block diagram of the control system is shown in Fig. 6. As will be explained in the next paragraphs, the control strategy designed uses feedback linearization to linearize only the kinematics, and uses internal loops to locally control the actuator's positions and velocities. This technique is an extension to the dynamic feedback linearization controller presented in Refs. [20–22], since we need to integrate the outputs from the nonlinear linearization law C_{FBL} . However, robustness is gained through the use of the internal loops.

In Fig. 6, the block *Kinematics* is represented by Eqs. (1)–(4), the process direction actuators, P_{p1} and P_{p2} by Eq. (5), and the steering actuators, P_{s1} and P_{s2} by Eq. (6). Furthermore, noticing that if we differentiate the output vector \underline{y} twice, we obtain

$$\ddot{y} = m(\underline{x}) + N(\underline{x}) \begin{bmatrix} \dot{\theta}_1 & \dot{\theta}_2 & \dot{\phi}_1 & \dot{\phi}_2 \end{bmatrix}^T \quad (7)$$

where $m(\underline{x})$ is a nonlinear 4×1 vector and $N(\underline{x})$ is a nonlinear 4×4 matrix; we design the following feedback linearization control law C_{FBL} :

$$\begin{bmatrix} \ddot{\theta}_{1d} & \ddot{\theta}_{2d} & \ddot{\phi}_{1d} & \ddot{\phi}_{2d} \end{bmatrix}^T = N^{-1}(\underline{x})(\underline{v}(\underline{x}) - m(\underline{x}))$$

$$\underline{v} = \begin{bmatrix} \ddot{x}_d + (K_x + \lambda_x)(\dot{x}_d - \dot{x}) + K_x \lambda_x (x_d - x) \\ \ddot{y}_d + (K_y + \lambda_y)(\dot{y}_d - \dot{y}) + K_y \lambda_y (y_d - y) \\ \ddot{\phi}_d + (K_\phi + \lambda_\phi)(\dot{\phi}_d - \dot{\phi}) + K_\phi \lambda_\phi (\phi_d - \phi) \\ \ddot{\delta}_d + (K_\delta + \lambda_\delta)(\dot{\delta}_d - \dot{\delta}) + K_\delta \lambda_\delta (\delta_d - \delta) \end{bmatrix} \quad (8)$$

where K and λ are the feedback linearization controller gains. We then use feedback plus feedforward to locally control the actuator's rotational velocities $\dot{\theta}_i$ and steering positions ϕ_i . These local controllers are given by

$$C_{FB_{pi}}(s) = \eta_{pi} + \frac{\gamma_{pi}}{s}; \quad C_{FF_{pi}}(s) = \frac{1}{\beta_{pi}} \left(1 + \frac{\alpha_{pi}}{s} \right) \quad (i=1,2)$$

$$C_{FB_{si}}(s) = \eta_{si} + \gamma_{pi}s; \quad C_{FF_{si}}(s) = \frac{1}{\beta_{si}} \left(1 + \frac{\alpha_{si}}{s} \right) \quad (i=1,2) \quad (9)$$

where η and γ are controller gains, and α and β are the actuator coefficients defined in Eqs. (5) and (6). As shown in Fig. 6, in order to use feedforward for steering position control, we estimate the steering acceleration $\ddot{\phi}_{id}$ through the use of a first order filter with gain τ_i ($i=1,2$). If τ_i is sufficiently small, the value of $\dot{\phi}_{id}$ will be very close to that of $\ddot{\phi}_i$. This technique, which is sometimes referred as dynamics surface control (DSC), has been proposed by Swaroop et al. [23]. Note that the success of the complete control strategy depends on the invertibility of matrix $N(x)$. It is shown in Refs. [15,16] that this matrix is invertible as long as the sheet always moves in the longitudinal direction ($\dot{\theta}_1, \dot{\theta}_2 \neq 0$).

5 Convergence Analysis of Closed-Loop System

In this section we will prove the local convergence of the control system described in Sec. 4 for a sheet of finite length by linearizing the system error dynamics. Thus, we will first set the error dynamics in terms of the paper and actuator errors as well as their corresponding surface errors. Then we will linearize the error dynamics around a predefined desired trajectory, and will show that, by proper selection of the controller gains, the error vector of the linearized control system converges asymptotically to zero. Let us first define paper coordinate errors and actuator errors by

$$\begin{aligned} \tilde{x} &= x_d - x, & \tilde{y} &= y_d - y \\ \tilde{\phi} &= \phi_d - \phi, & \tilde{\delta} &= \delta_d - \delta \\ \varepsilon_{pi} &= \dot{\theta}_{id} - \dot{\theta}_i, & \varepsilon_{si} &= \phi_{id} - \phi_i \quad (i=1,2) \\ \varepsilon_i &= \dot{\phi}_i - \dot{\phi}_{id} \quad (i=1,2) \end{aligned} \quad (10)$$

and let us also define the following surface errors:

$$\begin{aligned} s_x &= \dot{\tilde{x}} + \lambda_x \tilde{x}, & s_y &= \dot{\tilde{y}} + \lambda_y \tilde{y} \\ s_\phi &= \dot{\tilde{\phi}} + \lambda_\phi \tilde{\phi}, & s_\delta &= \dot{\tilde{\delta}} + \lambda_\delta \tilde{\delta} \\ s_{\varepsilon_{p1}} &= \dot{\varepsilon}_{p1} + \lambda_{\varepsilon_{p1}} \varepsilon_{p1}, & s_{\varepsilon_{p2}} &= \dot{\varepsilon}_{p2} + \lambda_{\varepsilon_{p2}} \varepsilon_{p2} \\ s_{\varepsilon_{s1}} &= \dot{\varepsilon}_{s1} + \lambda_{\varepsilon_{s1}} \varepsilon_{s1}, & s_{\varepsilon_{s2}} &= \dot{\varepsilon}_{s2} + \lambda_{\varepsilon_{s2}} \varepsilon_{s2} \end{aligned} \quad (11)$$

Combining now Eqs. (7), (8), and (10) we obtain the closed-loop expression

$$\ddot{y} = \underline{v}(\underline{x}) - N(\underline{x}) \begin{bmatrix} \dot{\varepsilon}_{p1} & \dot{\varepsilon}_{p2} & (\dot{\varepsilon}_{s1} + \varepsilon_1) & (\dot{\varepsilon}_{s2} + \varepsilon_2) \end{bmatrix}^T \quad (12)$$

If we further express $\underline{v}(\underline{x})$ from Eq. (8) in terms of paper and surface errors (Eqs. (10) and (11)), and let the actuator controller gains γ_{pi} and η_{si} in Eq. (9) be equal to

$$\gamma_{pi} = \frac{(\alpha_{pi} + \beta_{pi} \eta_{pi} - \lambda_{\varepsilon_{pi}}) \lambda_{\varepsilon_{pi}}}{\beta_{pi}} \quad (i=1,2)$$

$$\eta_{si} = \frac{(\alpha_{si} + \gamma_{si} \beta_{si} - \lambda_{\varepsilon_{si}}) \lambda_{\varepsilon_{si}}}{\beta_{si}} \quad (i=1,2) \quad (13)$$

the time derivatives of the errors in Eqs. (10) and (11) can be expressed as

$$\begin{aligned} \dot{\tilde{x}} &= -\lambda_x \tilde{x} + s_x \\ \dot{\tilde{y}} &= -\lambda_y \tilde{y} + s_y \\ \dot{\tilde{\phi}} &= -\lambda_\phi \tilde{\phi} + s_\phi \\ \dot{\tilde{\delta}} &= -\lambda_\delta \tilde{\delta} + s_\delta \\ \dot{\varepsilon}_{p1} &= -\lambda_{p1} \varepsilon_{p1} + s_{\varepsilon_{p1}} \\ \dot{\varepsilon}_{p2} &= -\lambda_{p2} \varepsilon_{p2} + s_{\varepsilon_{p2}} \\ \dot{\varepsilon}_{s1} &= -\lambda_{s1} \varepsilon_{s1} + s_{\varepsilon_{s1}} \\ \dot{\varepsilon}_{s2} &= -\lambda_{s2} \varepsilon_{s2} + s_{\varepsilon_{s2}} \\ \dot{s}_x &= -K_x s_x + n_{11} \dot{\varepsilon}_{p1} + n_{12} \dot{\varepsilon}_{p2} + n_{13} (\dot{\varepsilon}_{s1} + \varepsilon_1) + n_{14} (\dot{\varepsilon}_{s2} + \varepsilon_2) \\ \dot{s}_y &= -K_y s_y + n_{21} \dot{\varepsilon}_{p1} + n_{22} \dot{\varepsilon}_{p2} + n_{23} (\dot{\varepsilon}_{s1} + \varepsilon_1) + n_{24} (\dot{\varepsilon}_{s2} + \varepsilon_2) \\ \dot{s}_\phi &= -K_\phi s_\phi + n_{31} \dot{\varepsilon}_{p1} + n_{32} \dot{\varepsilon}_{p2} + n_{33} (\dot{\varepsilon}_{s1} + \varepsilon_1) + n_{34} (\dot{\varepsilon}_{s2} + \varepsilon_2) \\ \dot{s}_\delta &= -K_\delta s_\delta + n_{41} \dot{\varepsilon}_{p1} + n_{42} \dot{\varepsilon}_{p2} + n_{43} (\dot{\varepsilon}_{s1} + \varepsilon_1) + n_{44} (\dot{\varepsilon}_{s2} + \varepsilon_2) \\ \dot{s}_{\varepsilon_{p1}} &= -(\alpha_{p1} + \beta_{p1} \eta_{p1} - \lambda_{\varepsilon_{p1}}) s_{\varepsilon_{p1}} \\ \dot{s}_{\varepsilon_{p2}} &= -(\alpha_{p2} + \beta_{p2} \eta_{p2} - \lambda_{\varepsilon_{p2}}) s_{\varepsilon_{p2}} \\ \dot{s}_{\varepsilon_{s1}} &= -(\alpha_{s1} + \beta_{s1} \eta_{s1} - \lambda_{\varepsilon_{s1}}) s_{\varepsilon_{s1}} \\ \dot{s}_{\varepsilon_{s2}} &= -(\alpha_{s2} + \beta_{s2} \eta_{s2} - \lambda_{\varepsilon_{s2}}) s_{\varepsilon_{s2}} \end{aligned} \quad (14)$$

$$\begin{aligned} \dot{\varepsilon}_1 &= -\frac{1}{\tau_1} \varepsilon_1 + \frac{\dot{\tilde{\phi}}_1}{\delta \Psi} \dot{\Psi} + \frac{\dot{\delta \tilde{\phi}}_1}{\delta t} \\ \dot{\varepsilon}_2 &= -\frac{1}{\tau_2} \varepsilon_2 + \frac{\dot{\tilde{\phi}}_2}{\delta \Psi} \dot{\Psi} + \frac{\dot{\delta \tilde{\phi}}_2}{\delta t} \end{aligned} \quad (15)$$

where n_{ij} is the (i,j) element of matrix $N(\underline{x})$ in Eq. (7), and Ψ is defined by

$$\Psi = \begin{bmatrix} \tilde{x} & s_x & \tilde{y} & s_y & \tilde{\phi} & s_\phi & \tilde{\delta} & s_\delta \end{bmatrix}^T \quad (16)$$

If we now define the desired trajectory by

$$(x_d, y_d, \phi_d, \delta_d, \dot{x}_d, \dot{y}_d, \dot{\phi}_d, \dot{\delta}_d) = (0, \nu, 0, 0, 0, \nu, 0, 0) \quad (17)$$

where ν is the nominal longitudinal velocity of the sheet, and linearize the error dynamics in Eqs. (14) and (15) around $\tilde{x}=\tilde{y}=\tilde{\phi}=\tilde{\delta}=\varepsilon_{p1}=\varepsilon_{p2}=\varepsilon_{s1}=\varepsilon_{s2}=s_x=s_y=s_\phi=s_\delta=s_{\varepsilon_{p1}}=s_{\varepsilon_{p2}}=s_{\varepsilon_{s1}}=s_{\varepsilon_{s2}}=\varepsilon_1=\varepsilon_2=0$, we obtain an expression of the form

$$\dot{\underline{e}}(t) = G(t)\underline{e}(t) \quad (18)$$

where $\underline{e}(t)$ is the error vector, and it is defined by

$$\underline{e}(t) = [\bar{x} \quad \bar{y} \quad \bar{\phi} \quad \bar{\delta} \quad \bar{\varepsilon}_{p1} \quad \bar{\varepsilon}_{p2} \quad \bar{\varepsilon}_{s1} \quad \bar{\varepsilon}_{s2} \quad \bar{\varepsilon}]^T \quad (19)$$

whose elements are

$$\begin{aligned} \bar{x} &= \begin{bmatrix} \bar{x} \\ s_x \end{bmatrix}, \quad \bar{y} = \begin{bmatrix} \bar{y} \\ s_y \end{bmatrix}, \quad \bar{\phi} = \begin{bmatrix} \bar{\phi} \\ s_\phi \end{bmatrix} \\ \bar{\delta} &= \begin{bmatrix} \bar{\delta} \\ s_\delta \end{bmatrix}, \quad \bar{\varepsilon}_{p1} = \begin{bmatrix} \varepsilon_{p1} \\ s_{\varepsilon_{p1}} \end{bmatrix}, \quad \bar{\varepsilon}_{p2} = \begin{bmatrix} \varepsilon_{p2} \\ s_{\varepsilon_{p2}} \end{bmatrix} \\ \bar{\varepsilon}_{s1} &= \begin{bmatrix} \varepsilon_{s1} \\ s_{\varepsilon_{s1}} \end{bmatrix}, \quad \bar{\varepsilon}_{s2} = \begin{bmatrix} \varepsilon_{s2} \\ s_{\varepsilon_{s2}} \end{bmatrix}, \quad \bar{\varepsilon} = \begin{bmatrix} \varepsilon_1 \\ \varepsilon_2 \end{bmatrix} \end{aligned} \quad (20)$$

Similarly, the time-varying matrix $G(t)$ in Eq. (18) is given by

$$G(t) = \begin{bmatrix} A_x & 0 & 0 & 0 & B_x^{\varepsilon_{p1}}(t) & B_x^{\varepsilon_{p2}}(t) & B_x^{\varepsilon_{s1}} & 0 & B_x^\varepsilon \\ 0 & A_y & 0 & 0 & B_y^{\varepsilon_{p1}} & B_y^{\varepsilon_{p2}} & 0 & 0 & 0 \\ 0 & 0 & A_\phi & 0 & B_\phi^{\varepsilon_{p1}} & B_\phi^{\varepsilon_{p2}} & 0 & 0 & 0 \\ 0 & 0 & 0 & A_\delta & 0 & 0 & B_\delta^{\varepsilon_{s1}} & B_\delta^{\varepsilon_{s2}} & B_\delta^\varepsilon \\ 0 & 0 & 0 & 0 & A_{\varepsilon_{p1}} & 0 & 0 & 0 & 0 \\ 0 & 0 & 0 & 0 & 0 & A_{\varepsilon_{p2}} & 0 & 0 & 0 \\ 0 & 0 & 0 & 0 & 0 & 0 & A_{\varepsilon_{s1}} & 0 & 0 \\ 0 & 0 & 0 & 0 & 0 & 0 & 0 & A_{\varepsilon_{s2}} & 0 \\ B_\varepsilon^x & 0 & B_\varepsilon^\phi(t) & B_\varepsilon^\delta & B_\varepsilon^{\varepsilon_{p1}}(t) & B_\varepsilon^{\varepsilon_{p2}}(t) & B_\varepsilon^{\varepsilon_{s1}} & B_\varepsilon^{\varepsilon_{s2}} & A_\varepsilon \end{bmatrix} \quad (21)$$

whose matrix components are

$$\begin{aligned} A_x &= \begin{bmatrix} -\lambda_x & 1 \\ 0 & -K_x \end{bmatrix}, \quad A_y = \begin{bmatrix} -\lambda_y & 1 \\ 0 & -K_y \end{bmatrix} \\ A_\phi &= \begin{bmatrix} -\lambda_\phi & 1 \\ 0 & -K_\phi \end{bmatrix}, \quad A_\delta = \begin{bmatrix} -\lambda_\delta & 1 \\ 0 & -K_\delta \end{bmatrix} \\ A_{\varepsilon_{p1}} &= \begin{bmatrix} -\lambda_{\varepsilon_{p1}} & 1 \\ 0 & -g_{10,10} \end{bmatrix}, \quad A_{\varepsilon_{p2}} = \begin{bmatrix} -\lambda_{\varepsilon_{p2}} & 1 \\ 0 & -g_{12,12} \end{bmatrix} \\ A_{\varepsilon_{s1}} &= \begin{bmatrix} -\lambda_{\varepsilon_{s1}} & 1 \\ 0 & -g_{14,14} \end{bmatrix}, \quad A_{\varepsilon_{s2}} = \begin{bmatrix} -\lambda_{\varepsilon_{s2}} & 1 \\ 0 & -g_{16,16} \end{bmatrix} \\ A_\varepsilon &= \begin{bmatrix} -\lambda_{\varepsilon_1} & 0 \\ g_{18,17} & -\lambda_{\varepsilon_2} \end{bmatrix} \end{aligned} \quad (22)$$

$$\begin{aligned} B_x^{\varepsilon_{p1}}(t) &= \begin{bmatrix} 0 & 0 \\ g_{2,9} & g_{2,10} \end{bmatrix}, \quad B_x^{\varepsilon_{p2}}(t) = \begin{bmatrix} 0 & 0 \\ g_{2,11} & g_{2,12} \end{bmatrix} \\ B_x^{\varepsilon_{s1}} &= \begin{bmatrix} 0 & 0 \\ g_{2,13} & -\nu \end{bmatrix}, \quad B_x^\varepsilon = \begin{bmatrix} 0 & 0 \\ -\nu & 0 \end{bmatrix} \\ B_y^{\varepsilon_{p1}} &= \begin{bmatrix} 0 & 0 \\ g_{4,9} & g_{4,10} \end{bmatrix}, \quad B_y^{\varepsilon_{p2}} = \begin{bmatrix} 0 & 0 \\ g_{4,11} & g_{4,12} \end{bmatrix} \\ B_\phi^{\varepsilon_{p1}} &= \begin{bmatrix} 0 & 0 \\ g_{6,9} & g_{6,10} \end{bmatrix}, \quad B_\phi^{\varepsilon_{p2}} = \begin{bmatrix} 0 & 0 \\ g_{6,11} & g_{6,12} \end{bmatrix} \end{aligned}$$

$$B_\delta^{\varepsilon_{s1}} = \begin{bmatrix} 0 & 0 \\ g_{8,13} & \nu \end{bmatrix}, \quad B_\delta^{\varepsilon_{s2}} = \begin{bmatrix} 0 & 0 \\ g_{8,15} & -\nu \end{bmatrix}$$

$$B_\varepsilon^\phi = \begin{bmatrix} 0 & 0 \\ \nu & -\nu \end{bmatrix}, \quad B_\varepsilon^x = \begin{bmatrix} g_{17,1} & g_{17,2} \\ g_{18,1} & g_{18,2} \end{bmatrix}$$

$$B_\varepsilon^\phi(t) = \begin{bmatrix} g_{17,5} & g_{17,6} \\ g_{18,5} & g_{18,6} \end{bmatrix}, \quad B_\varepsilon^\delta = \begin{bmatrix} 0 & 0 \\ g_{18,7} & g_{18,8} \end{bmatrix}$$

$$B_\varepsilon^{\varepsilon_{p1}}(t) = \begin{bmatrix} g_{17,9} & g_{17,10} \\ g_{18,9} & g_{18,10} \end{bmatrix}, \quad B_\varepsilon^{\varepsilon_{p2}}(t) = \begin{bmatrix} g_{17,11} & g_{17,12} \\ g_{18,11} & g_{18,12} \end{bmatrix}$$

$$B_\varepsilon^{\varepsilon_{s1}} = \begin{bmatrix} g_{17,13} & g_{17,14} \\ g_{18,13} & g_{18,14} \end{bmatrix}, \quad B_\varepsilon^{\varepsilon_{s2}} = \begin{bmatrix} 0 & 0 \\ g_{18,15} & g_{18,16} \end{bmatrix} \quad (23)$$

Elements $g_{i,j}$, above, depend on system parameters and controller gains; elements $g_{2,9}$, $g_{2,10}$, $g_{2,11}$, $g_{2,12}$, $g_{17,3}$, $g_{17,9}$, $g_{17,10}$, $g_{17,11}$, $g_{17,12}$, $g_{18,5}$, $g_{18,6}$, $g_{18,9}$, $g_{18,10}$, $g_{18,11}$, and $g_{18,12}$ depend explicitly on time, and they do so linearly. This dependence on time comes from the definition of the desired trajectory of the sheet shown in Eq. (17).

In order to show the convergence of the control system errors, we will look at the dynamics of each of the elements of the error vector in Eq. (19), and will provide their algebraic solutions. Thus, combining Eqs. (19)–(23) we obtain the following expressions:

$$\dot{\bar{x}} = A_x \bar{x} + B_x^{\varepsilon_{p1}}(t) \bar{\varepsilon}_{p1} + B_x^{\varepsilon_{p2}}(t) \bar{\varepsilon}_{p2} + B_x^{\varepsilon_{s1}} \bar{\varepsilon}_{s1} + B_x^\varepsilon \bar{\varepsilon}$$

$$\dot{\bar{y}} = A_y \bar{y} + B_y^{\varepsilon_{p1}} \bar{\varepsilon}_{p1} + B_y^{\varepsilon_{p2}} \bar{\varepsilon}_{p2}$$

$$\dot{\bar{\phi}} = A_\phi \bar{\phi} + B_\phi^{\varepsilon_{p1}} \bar{\varepsilon}_{p1} + B_\phi^{\varepsilon_{p2}} \bar{\varepsilon}_{p2}$$

$$\dot{\bar{\delta}} = A_\delta \bar{\delta} + B_\delta^{\varepsilon_{s1}} \bar{\varepsilon}_{s1} + B_\delta^{\varepsilon_{s2}} \bar{\varepsilon}_{s2} + B_\delta^\varepsilon \bar{\varepsilon} \quad (24)$$

$$\dot{\bar{\varepsilon}}_{p1} = A_{\varepsilon_{p1}} \bar{\varepsilon}_{p1}$$

$$\dot{\bar{\varepsilon}}_{p2} = A_{\varepsilon_{p2}} \bar{\varepsilon}_{p2}$$

$$\dot{\bar{\varepsilon}}_{s1} = A_{\varepsilon_{s1}} \bar{\varepsilon}_{s1}$$

$$\dot{\bar{\varepsilon}}_{s2} = A_{\varepsilon_{s2}} \bar{\varepsilon}_{s2} \quad (25)$$

$$\begin{aligned} \dot{\bar{\varepsilon}} &= A_\varepsilon \bar{\varepsilon} + B_\varepsilon^x \bar{x} + B_\varepsilon^\phi(t) \bar{\phi} + B_\varepsilon^\delta \bar{\delta} + B_\varepsilon^{\varepsilon_{p1}}(t) \bar{\varepsilon}_{p1} + B_\varepsilon^{\varepsilon_{p2}}(t) \bar{\varepsilon}_{p2} + B_\varepsilon^{\varepsilon_{s1}} \bar{\varepsilon}_{s1} \\ &\quad + B_\varepsilon^{\varepsilon_{s2}} \bar{\varepsilon}_{s2} \end{aligned} \quad (26)$$

The solutions for ε_{pi} , ε_{si} , ($i=1,2$) can be easily obtained from Eq. (25) as follows:

$$\bar{\varepsilon}_{p1}(t) = e^{A_{\varepsilon_{p1}} t} \bar{\varepsilon}_{p1}(0)$$

$$\bar{\varepsilon}_{p2}(t) = e^{A_{\varepsilon_{p2}} t} \bar{\varepsilon}_{p2}(0)$$

$$\bar{\varepsilon}_{s1}(t) = e^{A_{\varepsilon_{s1}} t} \bar{\varepsilon}_{s1}(0)$$

$$\bar{\varepsilon}_{s2}(t) = e^{A_{\varepsilon_{s2}} t} \bar{\varepsilon}_{s2}(0) \quad (27)$$

Subsequently, the solutions for $\bar{x}(t)$, $\bar{y}(t)$, $\bar{\phi}(t)$, and $\bar{\delta}(t)$ can be obtained from Eqs. (24) and (27), and the solution for $\bar{\varepsilon}(t)$ from Eqs. (26) and (27) as

$$\begin{aligned}
\bar{x}(t) &= e^{A_x t} \bar{x}(0) + \left[\int_0^t e^{A_x(t-\tau)} B_x^{\varepsilon_{p1}}(\tau) e^{A_{\varepsilon_{p1}} \tau} d\tau \right] \bar{\varepsilon}_{p1}(0) \\
&+ \left[\int_0^t e^{A_x(t-\tau)} B_x^{\varepsilon_{p2}}(\tau) e^{A_{\varepsilon_{p2}} \tau} d\tau \right] \bar{\varepsilon}_{p2}(0) \\
&+ \left[\int_0^t e^{A_x(t-\tau)} B_x^{\varepsilon_{s1}} e^{A_{\varepsilon_{s1}} \tau} d\tau \right] \bar{\varepsilon}_{s1}(0) \\
&+ \left[\int_0^t e^{A_x(t-\tau)} B_x^{\varepsilon_{s2}} e^{A_{\varepsilon_{s2}} \tau} d\tau \right] \bar{\varepsilon}_{s2}(0) + \int_0^t e^{A_x(t-\tau)} B_x^{\varepsilon} \bar{\varepsilon}(\tau) d\tau \\
\bar{y}(t) &= e^{A_y t} \bar{y}(0) + \left[\int_0^t e^{A_y(t-\tau)} B_y^{\varepsilon_{p1}} e^{A_{\varepsilon_{p1}} \tau} d\tau \right] \bar{\varepsilon}_{p1}(0) \\
&+ \left[\int_0^t e^{A_y(t-\tau)} B_y^{\varepsilon_{p2}} e^{A_{\varepsilon_{p2}} \tau} d\tau \right] \bar{\varepsilon}_{p2}(0) \\
\bar{\phi}(t) &= e^{A_\phi t} \bar{\phi}(0) + \left[\int_0^t e^{A_\phi(t-\tau)} B_\phi^{\varepsilon_{p1}} e^{A_{\varepsilon_{p1}} \tau} d\tau \right] \bar{\varepsilon}_{p1}(0) \\
&+ \left[\int_0^t e^{A_\phi(t-\tau)} B_\phi^{\varepsilon_{p2}} e^{A_{\varepsilon_{p2}} \tau} d\tau \right] \bar{\varepsilon}_{p2}(0) \\
\bar{\delta}(t) &= e^{A_\delta t} \bar{\delta}(0) + \left[\int_0^t e^{A_\delta(t-\tau)} B_\delta^{\varepsilon_{s1}} e^{A_{\varepsilon_{s1}} \tau} d\tau \right] \bar{\varepsilon}_{s1}(0) \\
&+ \left[\int_0^t e^{A_\delta(t-\tau)} B_\delta^{\varepsilon_{s2}} e^{A_{\varepsilon_{s2}} \tau} d\tau \right] \bar{\varepsilon}_{s2}(0) + \int_0^t e^{A_\delta(t-\tau)} B_\delta^{\varepsilon} \bar{\varepsilon}(\tau) d\tau
\end{aligned} \tag{28}$$

$$\begin{aligned}
\bar{\varepsilon}(t) &= e^{A_\varepsilon t} \bar{\varepsilon}(0) + \int_0^t e^{A_\varepsilon(t-\tau)} B_\varepsilon^x(\tau) \bar{x}(\tau) d\tau + \int_0^t e^{A_\varepsilon(t-\tau)} B_\varepsilon^\phi(\tau) \bar{\phi}(\tau) d\tau \\
&+ \int_0^t e^{A_\varepsilon(t-\tau)} B_\varepsilon^\delta(\tau) \bar{\delta}(\tau) d\tau + \left[\int_0^t e^{A_\varepsilon(t-\tau)} B_\varepsilon^{\varepsilon_{p1}}(\tau) e^{A_{\varepsilon_{p1}} \tau} d\tau \right] \bar{\varepsilon}_{p1}(0) \\
&+ \left[\int_0^t e^{A_\varepsilon(t-\tau)} B_\varepsilon^{\varepsilon_{p2}}(\tau) e^{A_{\varepsilon_{p2}} \tau} d\tau \right] \bar{\varepsilon}_{p2}(0) \\
&+ \left[\int_0^t e^{A_\varepsilon(t-\tau)} B_\varepsilon^{\varepsilon_{s1}} e^{A_{\varepsilon_{s1}} \tau} d\tau \right] \bar{\varepsilon}_{s1}(0) \\
&+ \left[\int_0^t e^{A_\varepsilon(t-\tau)} B_\varepsilon^{\varepsilon_{s2}} e^{A_{\varepsilon_{s2}} \tau} d\tau \right] \bar{\varepsilon}_{s2}(0)
\end{aligned} \tag{29}$$

Finally, we can see from Eqs. (22), (23), and (27)–(29) that by proper selection of the controller gains, we can make matrices A_x , A_y , A_ϕ , A_δ , $A_{\varepsilon_{p1}}$, $A_{\varepsilon_{p2}}$, $A_{\varepsilon_{s1}}$, $A_{\varepsilon_{s2}}$, and A_ε Hurwitz, and thus $\bar{x}(t)$, $\bar{y}(t)$, $\bar{\phi}(t)$, $\bar{\delta}(t)$, $\bar{\varepsilon}_{p1}(t)$, $\bar{\varepsilon}_{p2}(t)$, $\bar{\varepsilon}_{s1}(t)$, $\bar{\varepsilon}_{s2}(t)$, and $\bar{\varepsilon}(t)$ will converge to zero asymptotically.

6 Controller Design Methodology

Since the page moves at a constant nominal longitudinal velocity, ν , the leading edge of the sheet will enter the ITS at a pre-specified time, T . Therefore, it is necessary to design a feedback system that will reduce all sheet positions and orientation errors to some pre-specified level within the allowable control time T . We will now state these control specifications more precisely as follows.

- i. The sheet has finite dimensions and moves with a nominal longitudinal velocity, ν .
- ii. The distance between the first and last optical sensors in Fig. 1 is given by L . Thus, the leading edge of the sheet will exit the steerable nip section at time $T=L/\nu$.
- iii. The sheet has maximum initial errors $\bar{x}_m(0)$, $\bar{y}_m(0)$, $\bar{\phi}_m(0)$, and $\bar{\delta}_m(0)$.
- iv. At time T , when the sheet exits the nip section, the maximum errors must be, respectively, smaller than or equal to $\bar{x}_m(T)$, $\bar{y}_m(T)$, $\bar{\phi}_m(T)$, and $\bar{\delta}_m(T)$.

Now, by looking at the expressions in Eqs. (27)–(29), we can develop a procedure to calculate the required controller gains for a sheet of finite dimensions moving at a prespecified nominal longitudinal velocity with some given initial and final state errors. Whereas the gains corresponding to $\bar{y}(t)$, $\bar{\phi}(t)$, $\bar{\varepsilon}_{pi}(t)$, and $\bar{\varepsilon}_{si}(t)$ ($i=1,2$) can be obtained directly, those corresponding to $\bar{x}(t)$, $\bar{\delta}(t)$, and $\bar{\varepsilon}(t)$ cannot, since the expressions for $\bar{x}(t)$ and $\bar{\delta}(t)$ depend on $\bar{\varepsilon}(t)$ and vice versa. Thus, we need to use the following iterative procedure.

- i. Given the initial and final maximum error bounds, $\varepsilon_{ji(m)}(0)$ and $\varepsilon_{ji(m)}(T)$, respectively, and their corresponding surface error bounds $s_{\varepsilon_{ji(m)}}(0)$ and $s_{\varepsilon_{ji(m)}}(T)$ for $j=s,p$ and $i=1,2$, use Eq. (27) to calculate the required controller gains $(\lambda_{\varepsilon_{pi}}, \eta_{\varepsilon_{pi}})$ and $(\lambda_{\varepsilon_{si}}, \gamma_{\varepsilon_{si}})$.
- ii. Given the initial maximum error bounds, $\bar{y}_m(0)$ and $\bar{\phi}_m(0)$, the final maximum error bounds, $\bar{y}_m(T)$ and $\bar{\phi}_m(T)$, their corresponding surface error bounds, $s_{y(m)}(0)$, $s_{\phi(m)}(0)$, $s_{y(m)}(T)$ and $s_{\phi(m)}(T)$, and the controller gains obtained in step (i), use the second and third expressions in Eq. (28) to calculate the required controller gains (λ_y, K_y) , and (λ_ϕ, K_ϕ) , respectively.
- iii. Given the initial and final maximum error bounds, $\varepsilon_{i(m)}(0)$ and $\varepsilon_{i(m)}(T)$, respectively, the controller gains obtained in steps (i) and (ii), and an initial guess for the controller gains (λ_x, K_x) and $(\lambda_\delta, K_\delta)$, use Eq. (29) to calculate the controller gains τ_i for $i=1,2$.
- iv. Given the initial maximum error bounds, $\bar{x}_m(0)$ and $\bar{\delta}_m(0)$, the final maximum error bounds, $\bar{x}_m(T)$ and $\bar{\delta}_m(T)$, the corresponding surface error bounds, $s_{x(m)}(0)$, $s_{\delta(m)}(0)$, $s_{x(m)}(T)$, and $s_{\delta(m)}(T)$, the controller gains initially guessed for (λ_x, K_x) and $(\lambda_\delta, K_\delta)$ in step (iii), and the controller gains obtained in steps (i)–(iii), use the first and fourth expressions in Eq. (28) to verify that the norms $|\bar{x}(T)|$ and $|\bar{\delta}(T)|$ are smaller than $\bar{x}_m(T)$ and $\bar{\delta}_m(T)$, respectively.
- v. Iterate between steps (iii) and (iv) if necessary.

As stated in step (v), even though this procedure requires some iteration, it should be noted that the initial guesses mentioned in step (iii) can be obtained from a simplified control system, which is described in Ref. [24]. The simplification consists in assuming that whereas we still control the velocity of the process direction motors through the internal loops shown in Fig. 6, inputs u_3 and u_4 are the steering angular velocities ($\dot{\phi}_1=u_3$; $\dot{\phi}_2=u_4$), which are obtained directly from the feedback linearization law in Eq. (8). They are then integrated once and fed directly as inputs to the kinematics block in Fig. 6. In this way, we would have inner loops for the process direction actuators, but not for the steering motors. Using these assumptions, the control gain synthesis problem is simplified not only because of the reduction in the inner loops, but also because we no longer need the first order filters shown in Fig. 6. The simplified system only has controller gains (λ_x, K_x) ,

Table 1 Maximum allowable initial and final state error bounds for simulation test. The unit for \tilde{x} , \tilde{y} , and $\tilde{\delta}$ is m; the unit for $\tilde{\phi}$, ϵ_{s1} , and ϵ_{s2} is rad; and the unit for ϵ_{p1} , ϵ_{p2} , ϵ_1 , and ϵ_2 is rad/s.

Initial errors	Final errors
$ \tilde{x}(0) \leq \tilde{x}_m(0) = 0.008$	$ \tilde{x}(T) \leq \tilde{x}_m(T) = 0.0013$
$ \tilde{y}(0) \leq \tilde{y}_m(0) = 0.040$	$ \tilde{y}(T) \leq \tilde{y}_m(T) = 0.0016$
$ \tilde{\phi}(0) \leq \tilde{\phi}_m(0) = 0.025$	$ \tilde{\phi}(T) \leq \tilde{\phi}_m(T) = 0.0035$
$ \tilde{\delta}(0) \leq \tilde{\delta}_m(0) = 0.0001$	$ \tilde{\delta}(T) \leq \tilde{\delta}_m(T) = 0.00002$
$\epsilon_{p1}(0) \leq \epsilon_{p1(m)}(0) = 0.1$	$\epsilon_{p1}(T) \leq \epsilon_{p1(m)}(T) = 0.01$
$\epsilon_{p2}(0) \leq \epsilon_{p2(m)}(0) = 0.1$	$\epsilon_{p2}(T) \leq \epsilon_{p2(m)}(T) = 0.01$
$\epsilon_{s1}(0) \leq \epsilon_{s1(m)}(0) = 0.1$	$\epsilon_{s1}(T) \leq \epsilon_{s1(m)}(T) = 0.01$
$\epsilon_{s2}(0) \leq \epsilon_{s2(m)}(0) = 0.1$	$\epsilon_{s2}(T) \leq \epsilon_{s2(m)}(T) = 0.01$
$\epsilon_1(0) \leq \epsilon_{1(m)}(0) = 0.1$	$\epsilon_1(T) \leq \epsilon_{1(m)}(T) = 0.01$
$\epsilon_2(0) \leq \epsilon_{2(m)}(0) = 0.1$	$\epsilon_2(T) \leq \epsilon_{2(m)}(T) = 0.01$

(λ_y, K_y) , (λ_ϕ, K_ϕ) , $(\lambda_\delta, K_\delta)$, $(\lambda_{\epsilon_{p1}}, \eta_{\epsilon_{p1}})$, and $(\lambda_{\epsilon_{p2}}, \eta_{\epsilon_{p2}})$, and they can be computed without any iteration. Furthermore, it should be noted that in most cases we only need one or two iterations between steps (iii) and (iv) before we arrive at the required controller gains for the desired specifications.

7 Simulation and Experimental Results

In order to determine the efficacy of the controller developed, we first performed simulation tests for a letter-sized sheet moving along the steerable nip section length, 0.2 m, at the nominal lon-

gitudinal velocity of 0.5 m/s from the initial to the final state errors shown in Table 1, where $T=0.42$ s represents the allowed time for control action.

Based on the initial and final maximum errors shown in Table 1 and the methodology presented in Sec. 6, the following controller gains were obtained: $(\lambda_x, K_x) = (80, 4.5)$, $(\lambda_y, K_y) = (80, 8.0)$, $(\lambda_\phi, K_\phi) = (80, 4.9)$, $(\lambda_\delta, K_\delta) = (95, 4.0)$, $(\lambda_{\epsilon_{p1}}, \eta_{\epsilon_{p1}}) = (100, 0.26)$, $(\lambda_{\epsilon_{p2}}, \eta_{\epsilon_{p2}}) = (100, 0.26)$, $(\lambda_{\epsilon_{s1}}, \gamma_{\epsilon_{s1}}) = (100, 9.31)$, $(\lambda_{\epsilon_{s2}}, \gamma_{\epsilon_{s2}}) = (100, 9.31)$, and $(\tau_1, \tau_2) = (0.0042, 0.0013)$. Figure 7 shows the simulation results using these controller gains. In this figure, the horizontal dotted lines mark the final state errors at the allowable control time, T , which is in term marked by the vertical dotted lines. It should be noticed the efficacy of the methodology presented in Sec. 6, since \tilde{x} , \tilde{y} , $\tilde{\phi}$, and $\tilde{\delta}$ are exactly reduced to the prescribed limits shown in Table 1 within the allowed control time.

Furthermore, we have also performed experimental tests in the system shown in Fig. 4. It should be noticed, however, that the actual experimental fixture cannot handle initial errors as large as those in Table 1 due to limitations in the setup design (range of the laser sensors for lateral and angular measurements in Fig. 1). Thus, based on the initial and final errors shown in Table 2 and the methodology presented in Sec. 6, the following controller gains were obtained: $(\lambda_x, K_x) = (80, 12.5)$, $(\lambda_y, K_y) = (80, 13.2)$, $(\lambda_\phi, K_\phi) = (80, 11.2)$, $(\lambda_\delta, K_\delta) = (80, 7.9)$, $(\lambda_{\epsilon_{p1}}, \eta_{\epsilon_{p1}}) = (100, 0.26)$, $(\lambda_{\epsilon_{p2}}, \eta_{\epsilon_{p2}}) = (100, 0.26)$, $(\lambda_{\epsilon_{s1}}, \gamma_{\epsilon_{s1}}) = (100, 9.31)$, $(\lambda_{\epsilon_{s2}}, \gamma_{\epsilon_{s2}}) = (100, 9.31)$, and $(\tau_1, \tau_2) = (0.0042, 0.0013)$. As shown in Fig. 8,

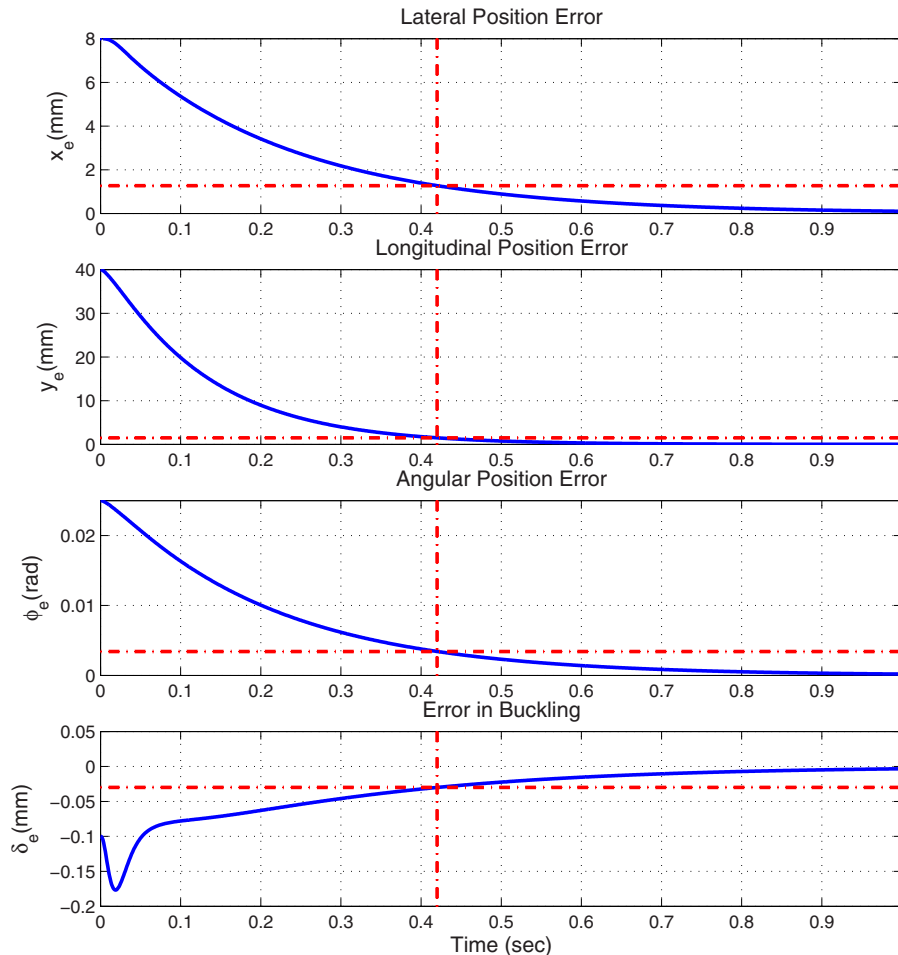


Fig. 7 Simulation results for large initial errors. The vertical dotted lines denote the allowable control time, T , and the horizontal lines denote the final errors at time T .

Table 2 Maximum allowable initial and final state error bounds for the experimental test. The unit for \tilde{x} , \tilde{y} , and $\tilde{\delta}$ is m; the unit for $\tilde{\phi}$, ϵ_{s1} , and ϵ_{s2} is rad; and the unit for ϵ_{p1} , ϵ_{p2} , ϵ_1 , and ϵ_2 is rad/s.

Initial errors	Final errors
$ \tilde{x}(0) \leq \tilde{x}_m(0) = 0.004$	$ \tilde{x}(T) \leq \tilde{x}_m(T) = 0.00026$
$ \tilde{y}(0) \leq \tilde{y}_m(0) = 0.0074$	$ \tilde{y}(T) \leq \tilde{y}_m(T) = 0.0005$
$ \tilde{\phi}(0) \leq \tilde{\phi}_m(0) = 0.025$	$ \tilde{\phi}(T) \leq \tilde{\phi}_m(T) = 0.001$
$ \tilde{\delta}(0) \leq \tilde{\delta}_m(0) = 0.0001$	$ \tilde{\delta}(T) \leq \tilde{\delta}_m(T) = 0.00002$
$ \epsilon_{p1}(0) \leq \epsilon_{p1(m)}(0) = 0.1$	$ \epsilon_{p1}(T) \leq \epsilon_{p1(m)}(T) = 0.01$
$ \epsilon_{p2}(0) \leq \epsilon_{p2(m)}(0) = 0.1$	$ \epsilon_{p2}(T) \leq \epsilon_{p2(m)}(T) = 0.01$
$ \epsilon_{s1}(0) \leq \epsilon_{s1(m)}(0) = 0.1$	$ \epsilon_{s1}(T) \leq \epsilon_{s1(m)}(T) = 0.01$
$ \epsilon_{s2}(0) \leq \epsilon_{s2(m)}(0) = 0.1$	$ \epsilon_{s2}(T) \leq \epsilon_{s2(m)}(T) = 0.01$
$ \epsilon_1(0) \leq \epsilon_{1(m)}(0) = 0.1$	$ \epsilon_1(T) \leq \epsilon_{1(m)}(T) = 0.01$
$ \epsilon_2(0) \leq \epsilon_{2(m)}(0) = 0.1$	$ \epsilon_2(T) \leq \epsilon_{2(m)}(T) = 0.01$

by using these controller gains, the system was able to reduce the sheet's initial position errors to prescribed levels in about 0.3 s. Note that the position increases constantly because the sheet moves in the longitudinal direction at all times. The discrepancies observed between simulation and experimental results can be attributed to sensor noise and model parameter uncertainties, such as friction coefficients. Particularly, Ergueta et al. [25] discussed the possible existence of unmodeled dynamics in the actuators, and presented a proof of the robustness of this control strategy to such uncertainties.

8 Conclusion

In this paper we have presented an innovative design that permits a swifter correction of lateral, longitudinal, and angular position errors in a paper path control system for xerographic and printing devices. This mechanism accomplished this task by having steerable nips.

In order to correct the sheet position errors we have used a controller based on dynamic feedback linearization [18,20–22] with the addition of internal loops for the control of the process direction velocity and steering position of the rollers; for these inner loops we have used feedback plus feedforward control.

In addition, not only have we provided a convergence analysis for the controller implemented, but also we have described a design methodology to determine the controller gains.

Simulation and experimental results show that by using the controller gains obtained from the methodology previously mentioned, it is possible to drive a sheet from an initial state with nonzero longitudinal velocity to a final state, also with nonzero longitudinal velocity in a very short time.

Acknowledgment

This work was supported by the National Science Foundation under Grant No. CMS 0301719, and by the financial support and collaboration with Xerox Corporation. In particular, the authors thank Dr. Martin Krucinski for his numerous critical remarks and suggestions during the development of this project.

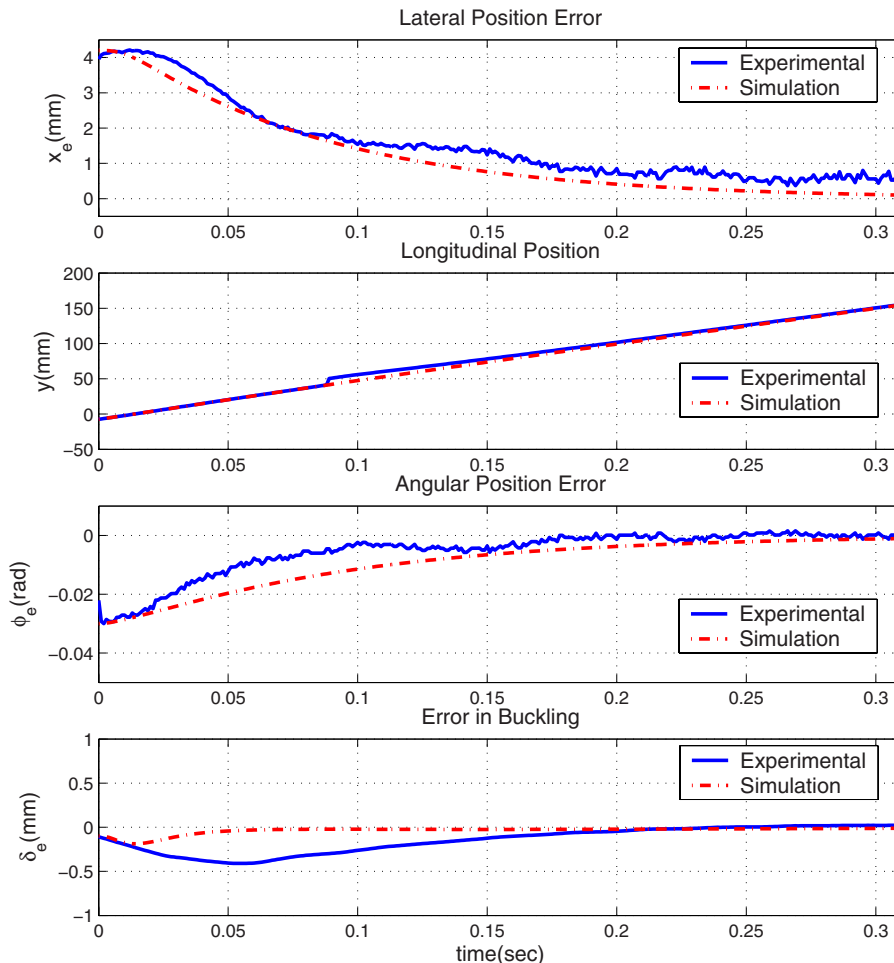


Fig. 8 Experimental and simulation results for small initial errors

References

- [1] Kruciński, M., Cloet, C., Horowitz, R., and Tomizuka, M., 1998, "Interobject Spacing Control and Controllability of a Manufacturing Transportation System," 1998 American Control Conference, Jun., Vol. 2, pp. 1259–1265, Session No. WA03-4.
- [2] Cloet, C., Kruciński, M., Horowitz, R., and Tomizuka, M., 1999, "A Hybrid Control Scheme for a Copier Paperpath," 1999 American Control Conference, San Diego, CA, Jun., Vol. 3, pp. 2114–2118.
- [3] Cloet, C., Kruciński, M., Horowitz, R., and Tomizuka, M., 1998, "Intersheet Spacing Control and Controllability of a Copier Paperpath," 1998 IEEE Conference on Control Applications, Trieste, Italy, Sept., Vol. 3, pp. 726–730.
- [4] Kruciński, M., Cloet, C., Horowitz, R., and Tomizuka, M., 2000, "A Mechatronics Approach to Copier Paperpath Control," First IFAC Conference on Mechatronic Systems, Darmstadt, Germany, Sept.
- [5] Krucinski, M., 2000, "Feedback Control of Photocopying Machinery," Ph.D. thesis, University of California, Berkeley, CA.
- [6] Cloet, C., 2001, "A Mechatronics Approach to Copier Paperpath Design," Ph.D. thesis, University of California, Berkeley, CA.
- [7] de Best, J. J. T. H., Bukkems, B. H. M., van de Molengraft, M. J. G., Heemels, W. P. M. H., and Steinbuch, M., 2008, "Robust Control of Piecewise Linear Systems: A Case Study in Sheet Flow Control," *Control Eng. Pract.*, **16**(8), pp. 991–1003.
- [8] Williams, L. A., deJong, J. N. M., Dondiego, M., and Savino, M. J., 1997, "Sheet Registration and Deskewing Device," U.S. Patent No. 5,678,159.
- [9] Lofthus, R. M., 1986, "Apparatus and Method for Combined Deskewing and Side Registering," U.S. Patent No. 4,971,304.
- [10] Kamprath, D. R., and Malachowski, M. A., 1990, "Translating Electronic Registration Systems," U.S. Patent No. 5,094,442.
- [11] Castelli, V. R., deJong, J. N. M., Williams, L. A., and Wolf, B. M., 1986, "Agile Lateral and Skew Sheet Registration Apparatus and Method," U.S. Patent No. 5,697,608.
- [12] Tanaka, N., Fukumoto, H., Arimoto, K., and Iwashita, Y., 1997, "Skew Correction Mechanism for Thermal Transfer Type Color Printers," International Conference on Micromechatronics for Information and Precision Equipment, Tokyo, Japan, Jul., pp. 635–638.
- [13] Hwang, S. S., 2002, "Sheet Registration and Deskewing System With Independent Drives and Steering," U.S. Patent No. 6,634,521.
- [14] Sanchez, R., Horowitz, R., and Tomizuka, M., 2004, "Paper Sheet Control Using Steerable Nips," 2004 American Control Conference Proceedings, Boston, MA, Jun. 30–Jul. 2, pp. 482–487.
- [15] Sanchez, R., Ergueta, E., Fine, B., Horowitz, R., Tomizuka, M., and Krucinskić, M., 2006, "A Mechatronic Approach to Full Sheet Control Using Steerable Nips," Fourth IFAC Symposium in Mechatronic Systems, Heidelberg, Germany, Sept. 12–15.
- [16] Sanchez, R., Horowitz, R., and Tomizuka, M., "Full Sheet Control Using a Steerable Nips Mechanism," *IEEE/ASME Trans. Mechatron.* (to be published).
- [17] Yun, X., and Sarkar, N., 1996, "Dynamic Feedback Control of Vehicles With Two Steerable Wheels," 1996 IEEE International Conference on Robotics and Automation, pp. 3105–3110.
- [18] Sastry, S. S., 1999, *Nonlinear Systems: Analysis, Stability, and Control*, Springer, New York.
- [19] Elliot, J. G., and Gans, R. F., 2008, "Closed-Loop Control of an Underactuated Sheet Registration Device Using Feedback Linearization and Gain Scheduling," *IEEE Trans. Control Syst. Technol.*, **16**, pp. 589–599.
- [20] Isidori, A., 1995, *Nonlinear Control Systems*, 3rd ed., Springer, New York.
- [21] Descusse, J., and Moog, C. H., 1985, "Decoupling With Dynamic Compensation for Strong Invertible Affine Non-Linear Systems," *Int. J. Control*, **42**(6), pp. 1287–1398.
- [22] d'Andrea Novel, B., Campion, G., and Bastin, G., 1995, "Control of Noholonomic Wheeled Mobile Robots by State Feedback Linearization," *Int. J. Robot. Res.*, **14**, pp. 543–559.
- [23] Swaroop, D., Gerdes, J. C., Yip, P. P., and Hedrick, J. K., 2000, "Dynamic Surface Control for a Class of Nonlinear Systems," *IEEE Trans. Autom. Control*, **45**(10), pp. 1893–1899.
- [24] Ergueta, E., Sanchez, R., Horowitz, R., and Tomizuka, M., 2007, "A Mechatronic Approach to Full Sheet Control Using Steer-Able Nips," ASME International Mechanical Engineering Congress and Exposition, Seattle, WA, Nov. 11–15.
- [25] Ergueta, E., Seifried, R., and Horowitz, R., 2008, "A Robust Approach to Dynamic Feedback Linearization for a Steerable Nips Mechanism," 2008 ASME Dynamic Systems and Control Conference, Ann Arbor, MI, Oct. 20–22.